nanomaterials

MDPI

Article

Stability of Coinage Metals Interacting with C_{60}

Navaratnarajah Kuganathan [1,2,*], Ratnasothy Srikaran [3] and Alexander Chroneos [1,2]

1 Department of Materials, Imperial College London, London SW7 2AZ, UK; alexander.chroneos@imperial.ac.uk
2 Faculty of Engineering, Environment and Computing, Coventry University, Priory Street, Coventry CV1 5FB, UK; ab8104@coventry.ac.uk
3 Department of Chemistry, University of Jaffna, Sir. Pon Ramanathan Road, Thirunelvely, Jaffna 40000, Srilanka; ratnasothysrikaran@gmail.com
* Correspondence: n.kuganathan@imperial.ac.uk or ad0636@coventry.ac.uk

Received: 27 September 2019; Accepted: 17 October 2019; Published: 18 October 2019

Abstract: Buckminsterfullerene (C_{60}) has been advocated as a perfect candidate material for the encapsulation and adsorption of a variety of metals and the resultant metallofullerenes have been considered for the use in different scientific, technological and medical areas. Using spin-polarized density functional theory together with dispersion correction, we examine the stability and electronic structures of endohedral and exohedral complexes formed between coinage metals (Cu, Ag and Au) and both non-defective and defective C_{60}. Encapsulation is exoergic in both forms of C_{60} and their encapsulation energies are almost the same. Exohedral adsorption of all three metals is stronger than that of endohedral encapsulation in the non-defective C_{60}. Structures and the stability of atoms interacting with an outer surface of a defective C_{60} are also discussed. As the atoms are stable both inside and outside the C_{60}, the resultant complexes can be of interest in different scientific and medical fields. Furthermore, all complexes exhibit magnetic moments, inferring that they can be used as spintronic materials.

Keywords: C_{60}; copper; silver; gold; encapsulation energy

1. Introduction

Buckminsterfullerene (C_{60}) is one of the allotropes of carbon exhibiting nanosized molecular structure with potential applications in chemistry, catalysis, material science, biology and medicine [1–8]. Encapsulation (atom located inside) and adsorption (atom located outside) of metal atoms have received great experimental and theoretical attention recently in order to optimise the application of C_{60}, mainly in catalytic processes, and electronic and metal storage devices [1–4,9–15].

A variety of metal atoms have been encapsulated within C_{60} experimentally for different applications [1–6]. The preparation of endohedral fullerenes can be mainly carried out by inserting metals, either during the preparation of fullerenes in the arc-vaporization technique [16] or after the preparation of fullerenes through five- or six-membered rings [17]. The latter method requires a high kinetic energy barrier as guest atoms need to travel through the five- or six-membered rings. There are other experimental methods available in the literature for the encapsulation [18–20]. A laser vaporization technique was used to encapsulate La by Klinger et al. [12] and the electronic behavior of the resultant compound was investigated using tunneling conductivity measurements. A recoil implantation technique was applied to encapsulate radioactive isotopes including ^{86}Zr and ^{168}Hf [17]. The resultant radioactive complexes were suggested for future applications in medical science as direct contact of toxic guest atoms with biological systems in the body can be avoided. Electronic structure calculations based on density functional theory (DFT) on several endohedral fullerenes have been reported in the literature [21–24]. Recently, we studied the thermodynamical stability and electronic

structures of volatile fission atoms (Xe, Kr, Br, I, Te, Rb and Cs) encapsulated within C_{60} using DFT simulation to predict the efficacy of C_{60} as a filter material in the spent fuel reprocessing [25].

Although there are many experimental studies available on endohedral fullerenes, only few experimental investigations have been reported on exohedral fullerenes [26–28]. Nevertheless, numerous theoretical simulations have been performed to study interactions of metal atoms on the surface of C_{60} [29–32]. Exohedral adsorption of a single atom and multiple atoms were studied by Sankar De et al. [29] using ab initio simulation in the absence of dispersion correction. In a very recent DFT simulation, we have shown the importance of dispersion correction for a Cd atom interacting with a C_{60} surface [33].

Encapsulation of coinage metals by C_{60} is of great interest as the resultant endohedral compounds can provide useful information about electronic structures of the encapsulated atoms required for the development of electronic materials. Huang et al. [34] synthesized Cu@C_{60} and its magnetic structure exhibits ring-current-induced magnetism. Experimental formation of Ag@C_{60} was reported by Narwade et al. [35] and its efficient electrocatalytic activity was tested in the fuel cell reaction. The growth of Au nanoparticles embedded in the C_{60} cage was experimentally characterised using a thermal co-evaporation technique by Singhal et al. [36]. Although there is an experimental interest in the literature, there are only few theoretical simulations of coinage metals interacting with C_{60}.

In the present study, we used DFT with dispersion correction to examine the stability of coinage metal atoms interacting (Cu, Ag and Au) both inside and outside non-defective and defective C_{60} molecules. The current simulation method enables the examination of the electronic structures, charge transfer and magnetic moment of the composites.

2. Computational Methods

All calculations were based on the DFT. The VASP code [37,38] which solves the Kohn–Sham (KS) equations using plane wave basis sets was used. The exchange correlation term was modelled using the generalized gradient approximation (GGA) with the Perdew, Burke and Ernzerhof (PBE) function [39]. A plane wave basis set with a cut-off value of 500 eV was used in all cases. Energy minimisation was performed using the conjugate gradient algorithm [40] with a force tolerance of 0.001 eV/Å. A single k-point (Γ) point was used in all calculations to represent the Brillouin zone due to the large supercell. Coinage bulk structures were optimised using a 16 × 16 × 16 Monkhorst k-point mesh [41] which yielded 64 k points. Cubic supercells with 20 Å were used in all calculations to ensure that the two adjacent images do not interact with each other. Encapsulation and adsorption energies were calculated using the following equation:

$$\text{Eenc/ads} = \text{E (M–C}_{60}\text{)} - \text{E (C}_{60}\text{)} - \text{E (M)}, \quad (1)$$

where E(C_{60}) is the total energy of non-defective or defective C_{60} molecule, E(M–C_{60}) is the total energy of a metal atom interacting with a non-defective or defective C_{60} and E (M) is the total energy of an isolated metal atom. Here, dispersive interaction was included by using the pair-wise force field as implemented by Grimme et al. [42] in the VASP package.

3. Results

3.1. Initial Configurations

Six different positions were considered for the interaction of coinage metals with C_{60}. At the endohedral position (endo), an atom occupies the center of a C_{60} molecule (refer to Figure 1). There are five different positions available on the outer surface of the C_{60} molecule for the adsorption of atoms, as shown in Figure 1. Positions "hex" and "pent" exhibit that the atom is just above the center of the hexagonal and pentagonal rings of the C_{60}, respectively. In the 66 and 65 configurations, the atom sits on the C–C bond, connecting two adjacent hexagonal rings and connecting one hexagonal and its nearest neighbor pentagonal ring, respectively. In the configuration "C", the metal atom is adsorbed by a C atom in the C_{60} cage.

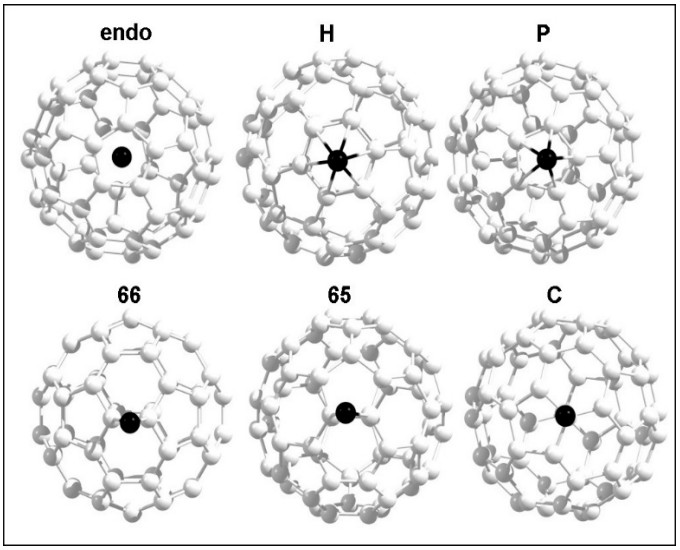

Figure 1. Initial configurations of a single metal atom interacting with a C_{60} molecule.

3.2. *Validation of the Pseudopotentials and Basis Sets*

In order to validate the choice of pseudopotentials and basis sets used in this study for C, Cu, Ag and Au, geometry optimisations were performed on a C_{60} molecule and bulk structures of coinage metals. Calculated geometrical parameters and electronic structures were then compared with corresponding experimental values and the values reported in other theoretical studies.

3.2.1. Calculation on Band Gap of a C_{60} Molecule

Geometry optimisation of a C_{60} molecule revealed bond length values of 1.45 Å and 1.40 Å for C−C and C=C, respectively. These values are in good agreement with the respective values of 1.43 Å and 1.39 Å reported experimentally [43]. The band gap was calculated by plotting the density of states (DOSs) and measuring the distance between the highest occupied molecular orbital (HOMO) and the lowest unoccupied molecular orbital (LUMO), as shown in the Figure 2. The estimated band gap value of 1.55 eV agrees well with the theoretical value of 1.64 eV [44]. Figure 2 shows the optimised structure of a C_{60} molecule together with its total DOS plot, HOMO and LUMO.

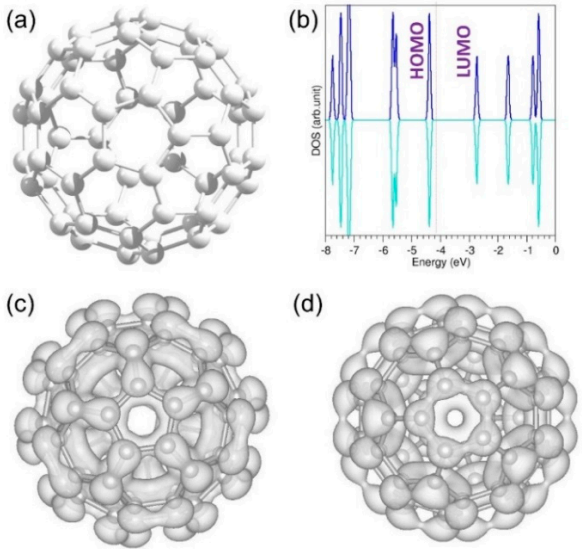

Figure 2. Relaxed structure (**a**), total density of state (DOS) (**b**), highest occupied molecular orbital (HOMO) (**c**), and lowest occupied molecular orbital (LUMO) (**d**) of a C_{60} molecule.

3.2.2. Calculations of Energy Minimisation on Bulk Cu, Ag and Au

Energy minimisation calculations were performed on bulk Cu, Ag and Au (*fcc* structure) structures to obtain equilibrium lattice constants and cohesive energies. Cohesive energy was calculated by considering the energy difference between an isolated gas-phase atom and an atom in the bulk. The calculated equilibrium lattice constants and cohesive energies (refer to Table 1) are in good agreement with the experimental and calculated values. Zero magnetic moments were calculated for all three bulk structures. DOS plots for the bulk structures of Cu, Ag and Au (refer to Figure 3) confirm the non-magnetic nature of bulk coinage metals. Considerable progress has recently been made on accurate theoretical determination of electronic band structure of solids. In order to describe the band structure of bulk copper, self-energy of d electrons was included in first-principles GW calculations by Marini et al. [45] and good agreement between experiment and theory was observed. In another theoretical study by Goraus et al. [46], on-site Coulomb interaction (U) was included for Ag 4d states in CeAgGa and the calculated density of states was in satisfactory agreement with X-ray photoemission spectra.

Table 1. Calculated and experimental lattice constants and cohesive energies of bulk coinage metals.

	Parameter					
	Lattice Constant (Å)			Cohesive Energy (eV)		
	Cu	**Ag**	**Au**	**Cu**	**Ag**	**Au**
Proposed method	3.57	4.09	4.12	3.99	2.97	3.63
Experiment	3.59 [47]	4.06 [47]	4.06 [47]	3.48 [48]	2.94 [48]	3.81 [48]
Other theory	3.501–3.686 [48]	4.046–4.321 [48]	4.084–4.112 [48]	2.54–4.42 [48]	1.87–3.60 [48]	2.23–3.86 [48]

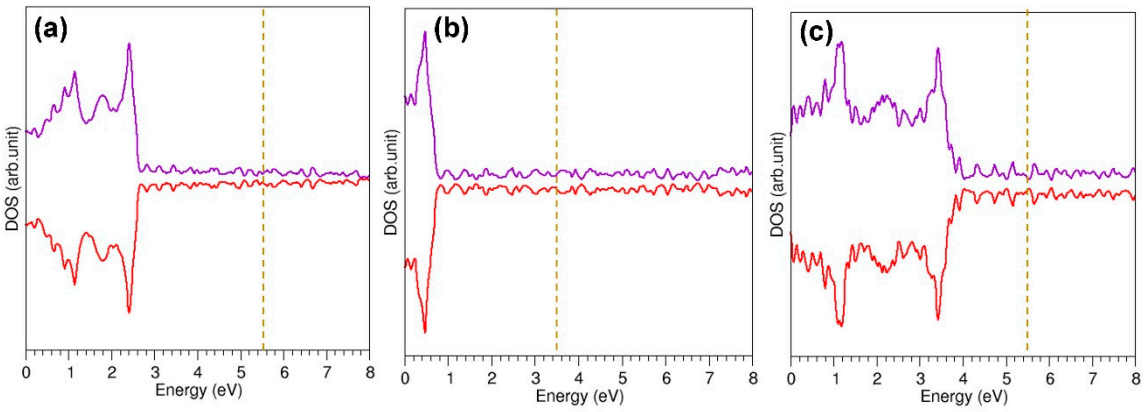

Figure 3. DOS plots for the bulk structures of Cu (**a**), Ag (**b**) and Au (**c**). Dotted lines correspond to the Fermi energy.

3.3. Encapsulation of Coinage Metals within C_{60}

First, the stability of a single coinage metal occupying the center of the cage was considered. Relaxed structures revealed that the encapsulated atoms (Cu, Ag and Au) are still in the center of the cage without altering their atomic positions. Encapsulation energy was calculated to determine the thermodynamical stability of the atoms when they are inside the C_{60}. The equation showing the methodology of calculating encapsulation energy was reported in the methodology section. Calculations were carried out with and without dispersion. Encapsulation energies calculated using dispersion are exoergic, meaning that they are stable inside the C_{60} (refer to Table 2). Endoergic encapsulation is observed in calculations without dispersion, inferring the importance of the dispersion. Enhancement in the encapsulation is due to the additional attractive term introduced by the dispersion. The rest of the calculations in this study were only performed with dispersion.

Both Cu and Au have similar encapsulation energies. This can be due to the identical empirical atomic radii of Cu and Au (1.35 Å) although their calculated values are 1.45 Å and 1.74 Å, respectively.

The calculated atomic radiis of Cu, Ag and Au are in ascending order. However, the encapsulation energy does not follow any trend with it. Bader charge analysis [49] shows that there is a small amount of charge transferred from metal atoms to the C_{60} cage. The outer electronic configuration of all three metal atoms is $d^{10}s^1$, meaning that the magnetic moment is one as there is an un-paired electron in the *s*-shell. The net magnetic moment of a C_{60} molecule is calculated to be zero. The magnetic moment of the resultant complex is ~1. This indicates that the electronic configuration of the metal is unaltered. This is further supported by the very small positive Bader charge on the metal atoms.

Figure 4 shows the calculated total and atomic DOS plots and partial charge density distribution around the encapsulated atoms. Encapsulation introduces extra peaks associated with *s* and *d* orbitals. In the case of Cu, there is a slight overlap between s and d states near the Fermi energy. The d states are further away (~3 eV) from the Fermi energy level while the s states are closer to it. Encapsulation of Au introduces the s states near the Fermi level and the d states are 2 eV away from it.

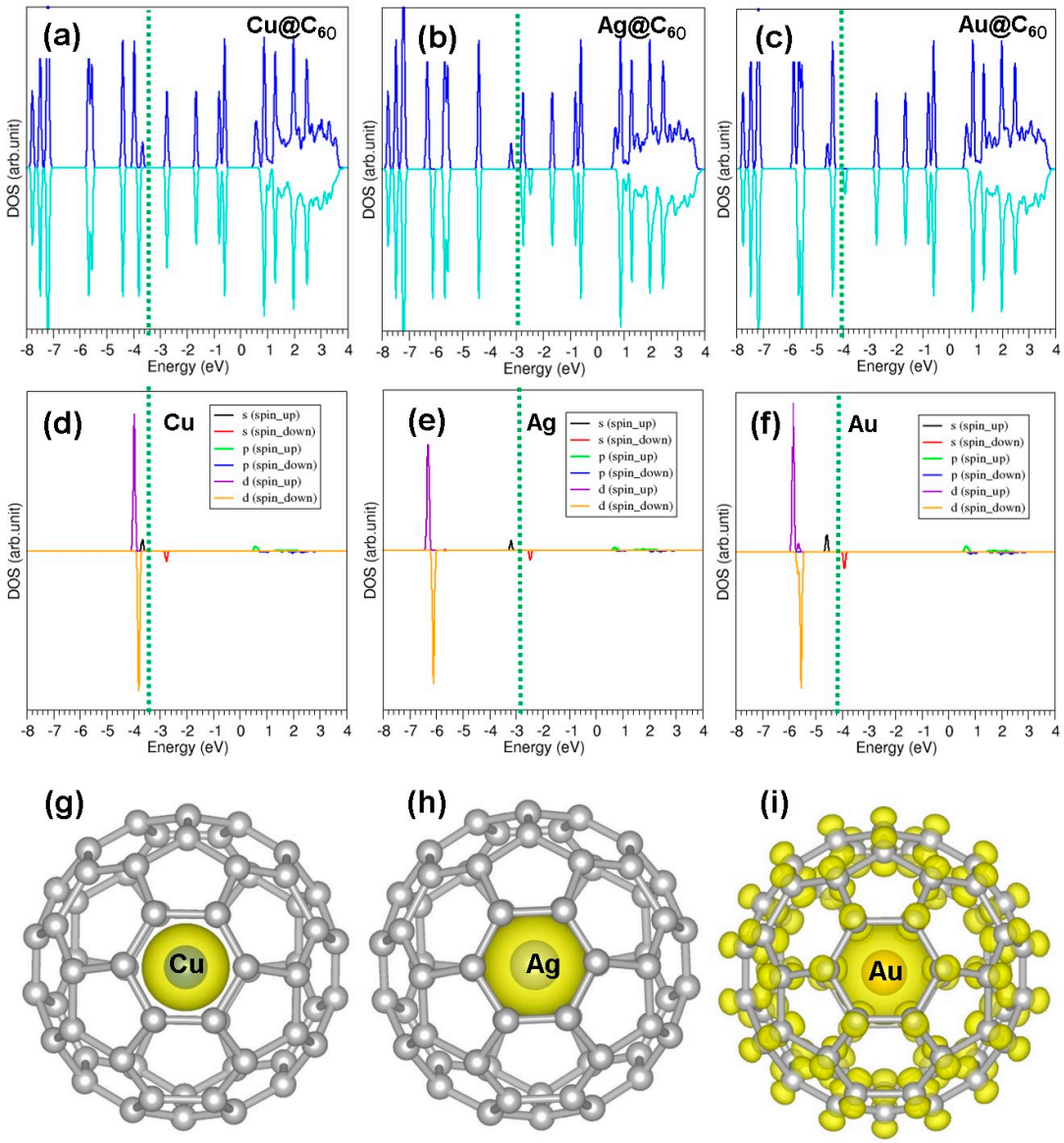

Figure 4. (**a**–**c**) Total DOSs for Cu, Ag and Au within a C_{60} molecule, respectively; (**d**–**f**) atomic doses for Cu, Ag and Au within a C_{60} molecule, respectively; and (**g**–**i**) charge density distributions around the encapsulated metal atoms for Cu, Ag and Au within a C_{60} molecule, respectively.

Table 2. Encapsulation energies of single coinage metal atoms incorporating the C_{60} molecule, Bader charges on metal atoms and magnetic moments of the resultant composites.

System	Atomic Radius (Å)		Encapsulation Energy (eV)		Bader Charge |e|		Magnetic Moment (μ)	
	Empirical [50]	Calculated [51]	DFT	DFT + D	DFT	DFT + D	DFT	DFT + D
$Cu@C_{60}$	1.35	1.45	0.13	**−0.58**	+0.1675	+0.1672	1.0000	1.0000
$Ag@C_{60}$	1.60	1.65	0.32	**−0.36**	+0.1704	+0.1701	0.9983	0.9983
$Au@C_{60}$	1.35	1.74	0.23	**−0.56**	+0.0956	+0.0954	0.9985	0.9985

3.4. Adsorption of Coinage Metals on the Surface of C_{60}

Here, we considered the adsorption of metal atoms by the outer surface of C_{60}. As discussed above, five different initial configurations were considered. Table 3 reports the final configurations and relative adsorption energies (refer to the methodology section for the equation that was used to calculate the adsorption energy) with respect to the most stable configuration.

Table 3. Initial and final configurations of coinage metal atoms adsorbed by the outer surface of the C_{60}.

Initial Configuration	Final Configuration and Relative Adsorption Energies (eV)		
	Cu	Ag	Au
H	C (0.00)	H (0.33)	H (0.67)
P	P (0.47)	P (0.30)	P (0.69)
66	66 (0.12)	C (0.00)	C (0.00)
65	65 (0.02)	65 (0.07)	C (0.00)
C	C (0.00)	C (0.00)	C (0.00)

The configuration "**C**" was found to be the most stable adsorption site and this is in agreement with the theoretical study reported by Shankar et al. [29]. Figure 5 shows the most stable geometries and bond distances formed between metal atoms and the C_{60}. Calculated adsorption energies are negative, meaning that all three metals are stable on the surface of the C_{60}. Copper forms a shorter Cu–C bond distance of 1.957 Å than the Ag–C_{60} and Au–C_{60} bond distances, which reflects in the adsorption energy and the Bader charge (refer to Table 4). The C–Ag bond distance is 2.242 Å which is slightly longer than the C–Cu and C–Au bond distances. The lower adsorption energy can be attributed to the longer C–Ag bond distance. In the case of Au, the adsorption energy is 0.09 eV less than that calculated for Cu. This is evidenced by the intermediate Au–C bond distance of 2.117 Å. Magnetic moments are not altered significantly. However, Bader charge and magnetic moment values are slightly higher and lower than that found in the encapsulated complexes, respectively, confirming the adsorption nature of atoms is stronger than encapsulation.

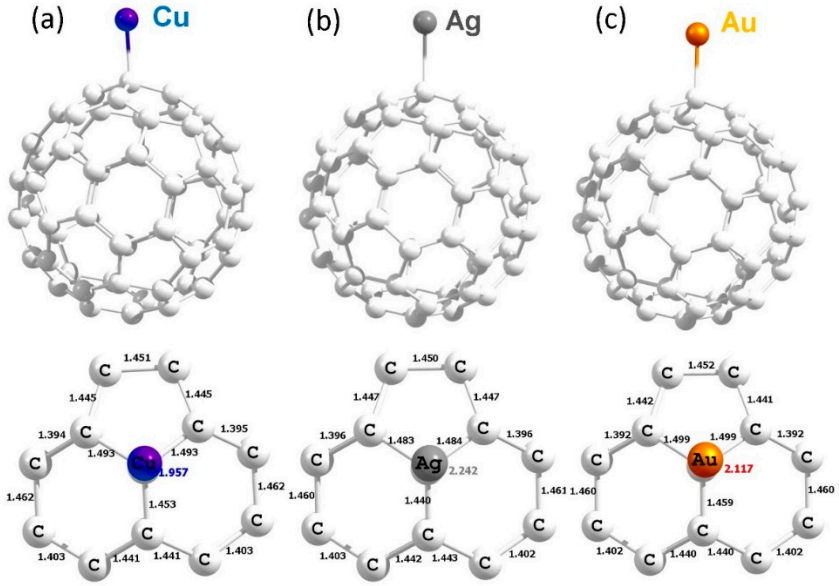

Figure 5. Optimised structures of Cu (**a**), Ag (**b**) and Au (**b**) adsorbed on the surface of C_{60}.

Figure 6 shows the total DOSs, atomic DOSs and charge density distribution plots showing the interaction of atoms with C_{60}. Additional states arising from *s* and *d* orbitals are introduced between the top of the valence band and bottom of the conduction band without altering the band gap significantly.

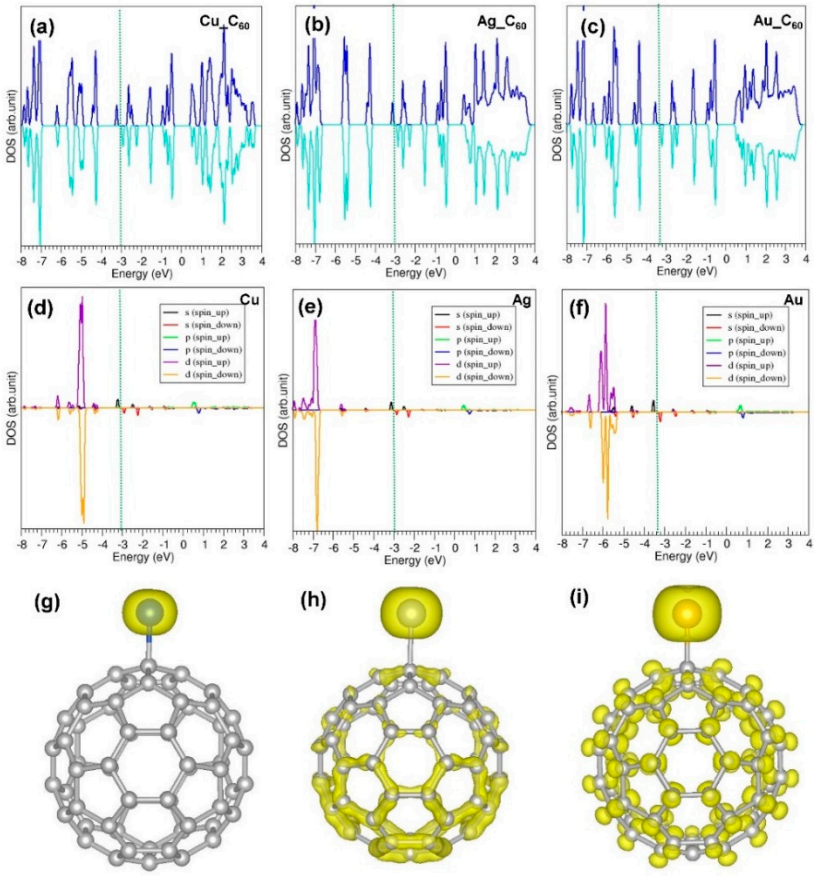

Figure 6. (**a**–**c**) Total DOSs for Cu, Ag and Au, respectively; (**d**–**f**) atomic doses for Cu, Ag and Au, respectively; and (**g**–**i**) charge density distributions around the adsorbed metal atoms for Cu, Ag and Au, respectively.

Table 4. Adsorption energies of atoms interacting with the surface of C_{60}, Bader charge on the metal atoms and magnetic moments of the composites.

System	Adsorption Energy (eV)	Bader Charge |e|	Magnetic Moment (μ)
Cu_C_{60}	−0.98	+0.30	0.9711
Ag_C_{60}	−0.50	+0.24	0.9329
Au_C_{60}	−0.89	+0.32	0.9778

3.5. Defective C_{60} Structure

Next, we considered a defective C_{60} structure to examine the encapsulation or adsorption capability of coinage metal atoms. A defect was introduced in C_{60} by removing a C atom. The relaxed structure, and DOS and charge density plots of defective C_{60} are shown in Figure 7. In previous experimental and theoretical studies, non-defective or defective single-walled nanotubes and C_{60} have been considered for the reaction with transition metals, molecules, one-dimensional crystals and metal clusters [52–57].

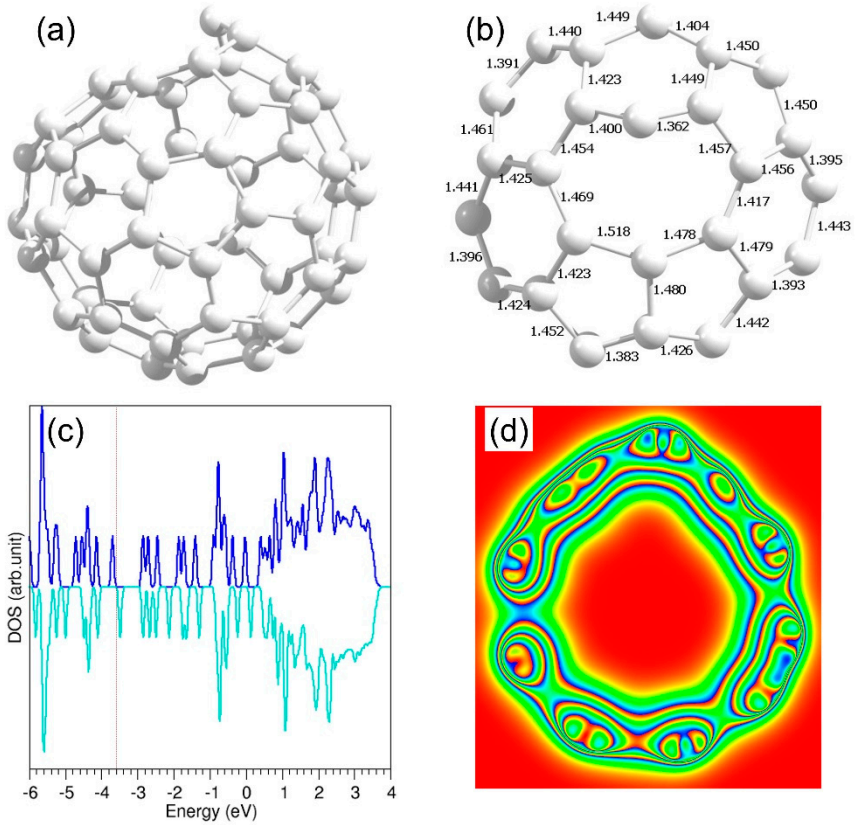

Figure 7. (**a**) Relaxed structure of a defective C_{60} molecule (**b**) bond distances around the defect (**c**) DOS and (**d**) cross sectional charge density plot.

The defective C_{60} structure forms an eight-membered ring with distorted C–C bond distances. The C_{60} molecule has now lost its symmetry and the outer surface of the optimised structure is expected to be more reactive with metal atoms. Furthermore, encapsulation via the eight-membered ring with larger open space can be easier than either a six- or a five-membered ring.

3.6. Encapsulation of Metal Atoms within a Defective C_{60} Molecule

In the optimised structures, the positions of the atoms are slightly deviated from the center of the cage and towards the defective part of the C_{60} molecule (refer to Figure 8). This is because of the non-symmetrical nature of the defective C_{60} molecule. The calculations show that the encapsulation

energies are exoergic, meaning that they are more stable in the cage of defective C_{60} molecule than in isolated atoms (refer to Table 5). Encapsulation energies are approximately −0.50 eV in all cases, indicating that interactions between metal atoms and the defective C_{60} molecule are almost the same. This is further supported by the similar C-M bond distances in the relaxed structures (refer to Figure 8). Bader charge analysis shows that metal atoms transfer a small amount of charge to C_{60}. The magnetic moment of the defective C_{60} molecule is zero. In all cases, magnetic moments of complexes are one, meaning that electronic configurations of coinage metal atoms are almost unaltered.

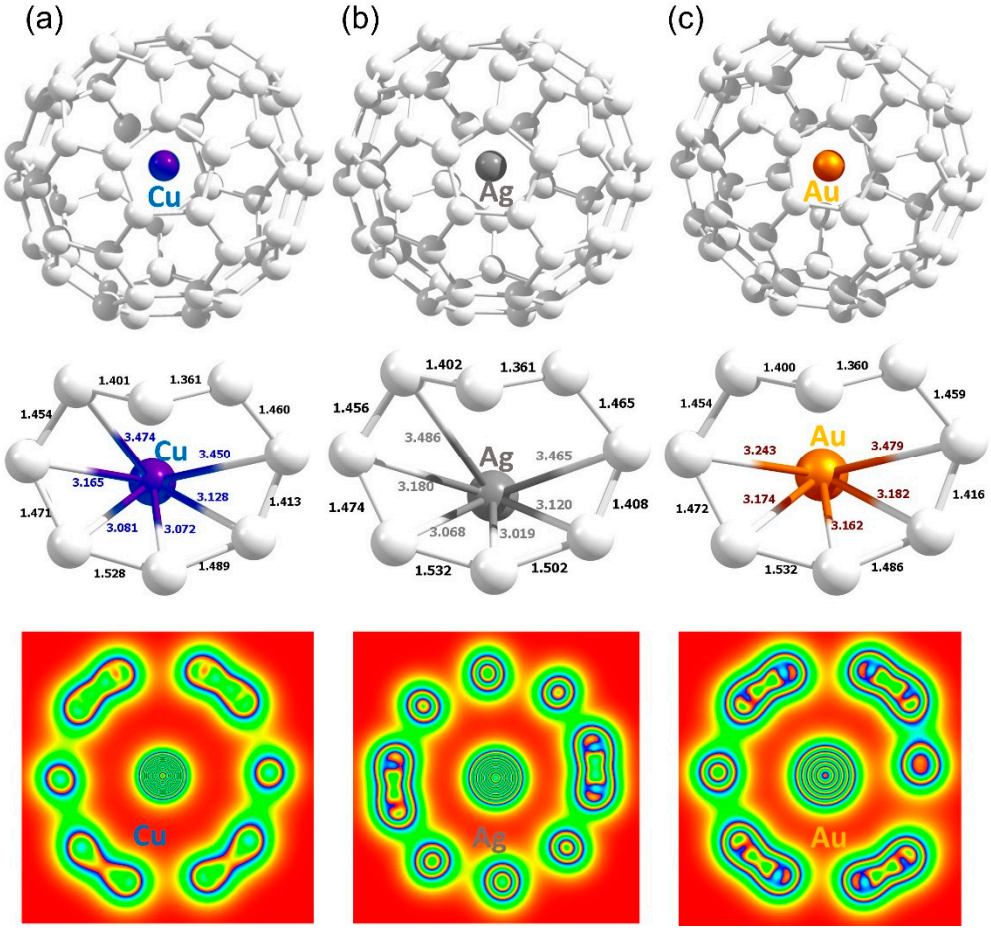

Figure 8. Relaxed structures and charge density plots of Cu (**a**), Ag (**b**) and Au (**c**) encapsulated within a defective C_{60} molecule.

Table 5. Encapsulation energies, Bader charge on the metal atoms and magnetic moments of the endohedral composites formed between the defective C_{60} molecule and metals.

System	Encapsulation Energy (eV)	Bader Charge |e|	Magnetic Moment (μ)
$Cu@C_{60\_defe}$	−0.56	+0.27	1.000
$Ag@C_{60\_defe}$	−0.43	+0.49	1.000
$Au@C_{60\_defe}$	−0.51	+0.31	1.000

3.7. Adsorption of Metal Atoms on the Surface of Defective C_{60} Molecule

Finally, interactions between atoms and defective surface of C_{60} were considered. There is a strong interaction between defect and metal atoms (refer to Figure 9). Metal atoms occupy the vacant side forming strong bonds with adjacent carbon atoms. This is evidenced by the bond distances, the amount of charge transferred (refer to Table 6), charge density plots and the reduction in the magnetic moments.

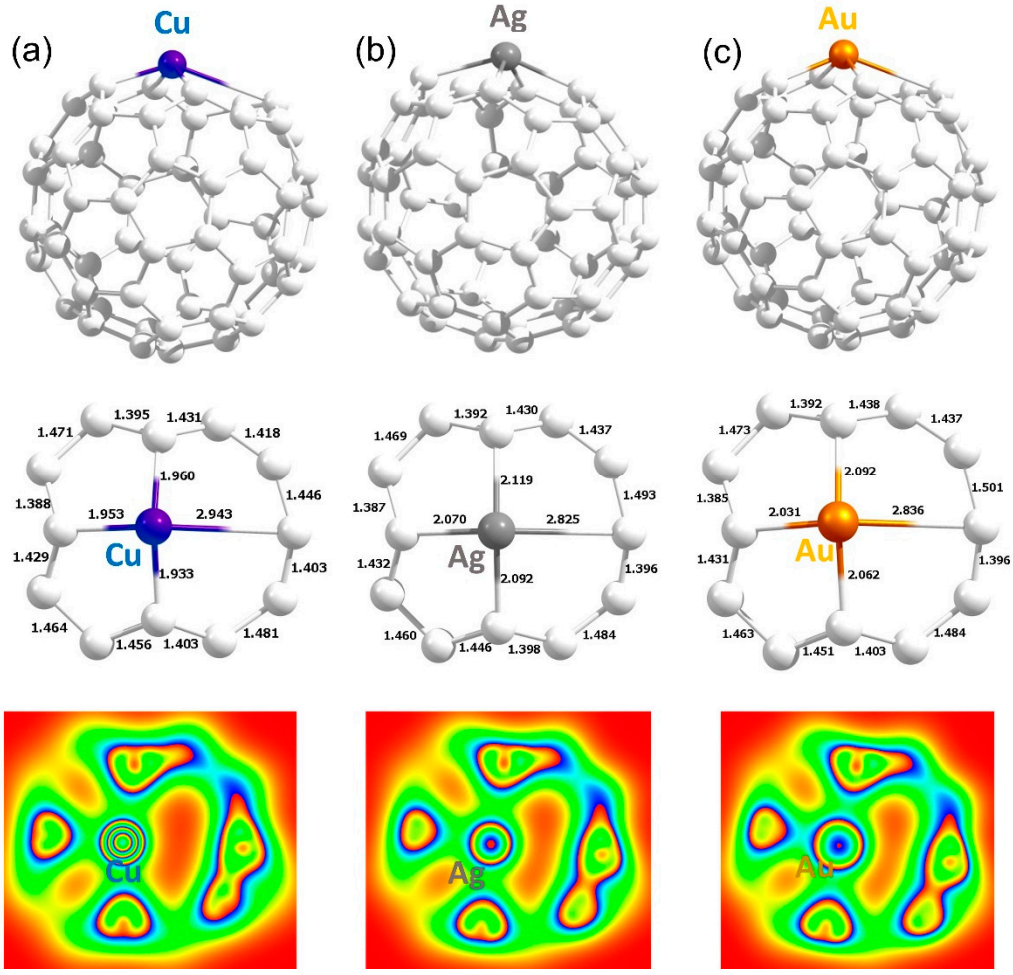

Figure 9. Relaxed structures and charge density plots of Cu (**a**), Ag (**b**) and Au (**c**) adsorbed on the surface of defective C_{60} molecule.

Table 6. Encapsulation energies, Bader charge on the metal atoms and magnetic moments of the composites formed between the surface of defective C_{60} molecule and metals.

System	Encapsulation Energy (eV)	Bader Charge |e|	Magnetic Moment (μ)
$Cu\_C_{60\_defe}$	−0.61	+0.70	0.8896
$Ag\_C_{60\_defe}$	−0.41	+0.62	0.9012
$Au\_C_{60\_defe}$	−0.48	+0.51	0.9414

4. Conclusions

In this study, DFT simulations, together with dispersion correction, were performed to examine the encapsulation and adsorption capability of both non-defective and defective C_{60} molecules. Calculations show that the non-defective C_{60} can trap all three metals both endohedrally and exohedrally. Significant enhancement is observed for the exohedral adsorption compared to for the endohedral encapsulation in the non-defective C_{60}. Furthermore, the defective C_{60} was examined for trapping both endohedrally and exohedrally. Encapsulation and adsorption energies are exoergic, suggesting that the defective C_{60} is also a candidate host material for trapping coinage metals. Both non-defective and defective C_{60} structures can be ideal host materials in scientific and medical fields. As resultant M–C_{60} complexes are magnetic, they can play an important role in spintronic devices.

Author Contributions: Computation, N.K.; writing of original draft preparation, N.K.; writing of review and editing, R.S. and A.C.

Funding: This research received no external funding.

Acknowledgments: The High Performance Computing (HPC) Center at Imperial College London is acknowledged for providing computational facilities and technical support.

Conflicts of Interest: The authors declare no conflicts of interest.

References

1. Kroto, H.W.; Allaf, A.W.; Balm, S.P. C_{60}: Buckminsterfullerene. *Chem. Rev.* **1991**, *91*, 1213–1235. [CrossRef]
2. Popov, A.A.; Yang, S.; Dunsch, L. Endohedral Fullerenes. *Chem. Rev.* **2013**, *113*, 5989–6113. [CrossRef]
3. Acquah, S.; Penkova, A.V.; Markelov, D.; Semisalova, A.S.; Leonhardt, B.E.; Magi, J.M. Review—The Beautiful Molecule: 30 Years of C_{60} and Its Derivatives. *ECS J. Solid State Sci. Technol.* **2017**, *6*, M3155–M3162.
4. Bühl, M.; Hirsch, A. Spherical Aromaticity of Fullerenes. *Chem. Rev.* **2001**, *101*, 1153–1184. [CrossRef] [PubMed]
5. Dresselhaus, M.S.; Dresslhaus, G. Fullerenes and Fullerene Derived Solids as Electronic Materials. *Annu. Rev. Mater. Sci.* **1995**, *25*, 487–523. [CrossRef]
6. Bakry, R.; Vallant, R.M.; Najam-ul-Haq, M.; Rainer, M.; Szabo, Z.; Huck, C.W.; Bonn, G.K. Medicinal applications of fullerenes. *Int. J. Nanomed.* **2007**, *2*, 639–649.
7. Goodarzi, S.; Da Ros, T.; Conde, J.; Sefat, F.; Mozafari, M. Fullerene: Biomedical engineers get to revisit an old friend. *Mater. Today* **2017**, *20*, 460–480. [CrossRef]
8. Kroto, H.W. C_{60}: Buckminsterfullerene, The Celestial Sphere that Fell to Earth. *Angew. Chem. Int. Ed. Engl.* **1992**, *31*, 111–129. [CrossRef]
9. He, T.; Gao, G.; Kou, L.; Will, G.; Du, A. Endohedral metallofullerenes ($M@C_{60}$) as efficient catalysts for highly active hydrogen evolution reaction. *J. Catal.* **2017**, *354*, 231–235. [CrossRef]
10. Mahdy, A.M.E. DFT study of hydrogen storage in Pd-decorated C60 fullerene. *Mol. Phys.* **2015**, *113*, 3531–3544. [CrossRef]
11. Tawfik, S.A.; Cui, X.Y.; Ringer, S.P.; Stampfl, C. Endohedral metallofullerenes, $M@C_{60}$ (M = Ca, Na, Sr): Selective adsorption and sensing of open-shell NOx gases. *Phys. Chem. Chem. Phys.* **2016**, *18*, 21315–21321. [CrossRef] [PubMed]
12. Klingeler, R.; Kann, G.; Wirth, I.; Eisebitt, S.; Bechthold, P.S.; Neeb, M.; Eberhardt, W. $La@C_{60}$: A metallic endohedral fullerene. *J. Chem. Phys.* **2001**, *115*, 7215–7218. [CrossRef]
13. Cho, S.C.; Kaneko, T.; Ishida, H.; Hatakeyama, R. Nitrogen-atom endohedral fullerene synthesis with high efficiency by controlling plasma-ion irradiation energy and C_{60} internal energy. *J. Appl. Phys.* **2015**, *117*, 123301. [CrossRef]
14. Ohtsuki, T.; Masumoto, K.; Ohno, K.; Maruyma, Y.; Kawazoe, Y.; Sueki, K.; Kikuchi, K. Insertion of Be Atoms in C_{60} Fullerene Cages: $Be@C_{60}$. *Phys. Rev. Lett.* **1996**, *77*, 3522–3524. [CrossRef]
15. Kuganathan, N.; Green, J.C.; Himmel, H.-J. Dinitrogen fixation and activation by Ti and Zr atoms, clusters and complexes. *New J. Chem.* **2006**, *30*, 1253–1262. [CrossRef]
16. Kyesmen, P.I.; Onoja, A.; Amah, A.N. Fullerenes synthesis by combined resistive heating and arc discharge techniques. *Springerplus* **2016**, *5*, 1323. [CrossRef]
17. Saha, S.K.; Chowdhury, D.P.; Das, S.K.; Guin, R. Encapsulation of radioactive isotopes into C_{60} fullerene cage by recoil implantation technique. *Nucl. Instrum. Methods Phys. Res. Sect. B Beam Interact. Mater. Atoms* **2006**, *243*, 277–281. [CrossRef]
18. Wan, Z.; Christian, J.F.; Anderson, S.L. Collision of Li^+ and Na^+ with C_{60}: Insertion, fragmentation, and thermionic emission. *Phys. Rev. Lett.* **1992**, *69*, 1352–1355. [CrossRef]
19. Saunders, M.; Cross, R.J.; Jiménez-Vázquez, H.A.; Shimshi, R.; Khong, A. Noble gas atoms inside fullerenes. *Science* **1996**, *271*, 1693–1697. [CrossRef]
20. Braun, T.; Rausch, H. Endohedral incorporation of argon atoms into C_{60} by neutron irradiation. *Chem. Phys. Lett.* **1995**, *237*, 443–447. [CrossRef]
21. Brocławik, E.; Eilmes, A. Density functional study of endohedral complexes $M@C_{60}$ (M=Li, Na, K, Be, Mg, Ca, La, B, Al): Electronic properties, ionization potentials, and electron affinities. *J. Chem. Phys.* **1998**, *108*, 3498–3503. [CrossRef]

22. Srivastava, A.K.; Pandey, S.K.; Misra, N. Encapsulation of lawrencium into C_{60} fullerene: Lr@C_{60} versus Li@C_{60}. *Mater. Chem. Phys.* **2016**, *177*, 437–441. [CrossRef]
23. Wang, Y.; Tománek, D.; Ruoff, R.S. Stability of M@C60 endohedral complexes. *Chem. Phys. Lett.* **1993**, *208*, 79–85. [CrossRef]
24. Lu, J.; Zhang, X.; Zhao, X. Electronic structures of endohedral N@C_{60}, O@C_{60} and F@C_{60}. *Chem. Phys. Lett.* **1999**, *312*, 85–90. [CrossRef]
25. Kuganathan, N.; Arya, A.K.; Rushton, M.J.D.; Grimes, R.W. Trapping of volatile fission products by C_{60}. *Carbon* **2018**, *132*, 477–485. [CrossRef]
26. Breton, J.; Gonzalez-Platas, J.; Girardet, C. Endohedral and exohedral adsorption in C_{60}: An analytical model. *J. Chem. Phys.* **1993**, *99*, 4036–4040. [CrossRef]
27. Yekymov, E.; Bounioux, C.; Itzhak-Cohen, R.; Zeiri, L.; Shahnazaryan, E.; Katz, E.A.; Yerushalmi-Rozen, R. All carbon non-covalent exohedral hybrids: C_{60} aggregates on nanotube networks. *J. Energy Chem.* **2018**, *27*, 957–961. [CrossRef]
28. Nakamura, Y.; Kato, S.-I. Exohedral functionalization of fullerenes and supramolecular chemistry. *Chem. Rec.* **2011**, *11*, 77–94. [CrossRef]
29. Sankar De, D.; Flores-Livas, J.A.; Saha, S.; Genovese, L.; Goedecker, S. Stable structures of exohedrally decorated C_{60}-fullerenes. *Carbon* **2018**, *129*, 847–853. [CrossRef]
30. Özdamar, B.; Boero, M.; Massobrio, C.; Felder-Flesch, D.; Roux, S.L. Exohedral M–C_{60} and M_2–C_{60} (M = Pt, Pd) systems as tunable-gap building blocks for nanoarchitecture and nanocatalysis. *J. Chem. Phys.* **2015**, *143*, 114308. [CrossRef]
31. Kobayashi, T.; Yokoyama, K. Theoretical study of the adsorption of Cs, Cs+, I, I−, and CsI on C_{60} fullerene. *J. Nucl. Sci. Technol.* **2016**, *53*, 1489–1493. [CrossRef]
32. Suzumura, J.-i.; Hosoya, N.; Nagao, S.; Mitsui, M.; Nakajima, A. Electronic structures of exohedral lanthanide-C_{60} clusters. *J. Chem. Phys.* **2004**, *121*, 2649–2654. [CrossRef] [PubMed]
33. Kuganathan, N.; Selvanantharajah, N.; Iyngaran, P.; Abiman, P.; Chroneos, A. Cadmium trapping by C_{60} and B-, Si-, and N-doped C_{60}. *J. Appl. Phys.* **2019**, *125*, 054302. [CrossRef]
34. Huang, H.; Ata, M.; Yoshimoto, Y. Cu@C_{60} formation in rf-plasma and ring-current induced magnetism of C_{60}. *Chem. Commun.* **2004**, *10*, 1206–1207. [CrossRef]
35. Narwade, S.S.; Mulik, B.B.; Mali, S.M.; Sathe, B.R. Silver nanoparticles sensitized C_{60}(Ag@C_{60}) as efficient electrocatalysts for hydrazine oxidation: Implication for hydrogen generation reaction. *Appl. Surf. Sci.* **2017**, *396*, 939–944. [CrossRef]
36. Singhal, R.; Sharma, P.; Vishnoi, R.; Avasthi, D.K. Synthesis and characterizations of Au-C_{60} nanocomposite. *J. Alloys Compd.* **2017**, *696*, 9–15. [CrossRef]
37. Kresse, G.; Furthmüller, J. Efficient iterative schemes for ab initio total-energy calculations using a plane-wave basis set. *Phys. Rev. B* **1996**, *54*, 11169–11186. [CrossRef]
38. Kresse, G.; Joubert, D. From ultrasoft pseudopotentials to the projector augmented-wave method. *Phys. Rev. B* **1999**, *59*, 1758–1775. [CrossRef]
39. Perdew, J.P.; Burke, K.; Ernzerhof, M. Generalized Gradient Approximation Made Simple. *Phys. Rev. Lett.* **1996**, *77*, 3865–3868. [CrossRef]
40. Press, W.H.; Teukolsky, S.A.; Vetterling, W.T.; Flannery, B.P. *Numerical Recipes in C: The Art of Scientific Computing*, 2nd ed.; Cambridge University Press: Cambridge, UK, 1992; p. 994.
41. Monkhorst, H.J.; Pack, J.D. Special points for Brillouin-zone integrations. *Phys. Rev. B* **1976**, *13*, 5188–5192. [CrossRef]
42. Grimme, S.; Antony, J.; Ehrlich, S.; Krieg, H. A consistent and accurate ab initio parametrization of density functional dispersion correction (DFT-D) for the 94 elements H-Pu. *J. Chem. Phys.* **2010**, *132*, 154104. [CrossRef] [PubMed]
43. Hawkins, J.M. Osmylation of C_{60}: Proof and characterization of the soccer-ball framework. *Acc. Chem. Res.* **1992**, *25*, 150–156. [CrossRef]
44. Goclon, J.; Winkler, K.; Margraf, J.T. Theoretical investigation of interactions between palladium and fullerene in polymer. *RSC Adv.* **2017**, *7*, 2202–2210. [CrossRef]
45. Marini, A.; Onida, G.; Del Sole, R. Quasiparticle Electronic Structure of Copper in the GW Approximation. *Phys. Rev. Lett.* **2001**, *88*, 016403. [CrossRef] [PubMed]

46. Goraus, J.; Ślebarski, A.; Fijałkowski, M. Electronic structure of CeAgGa based on the experimental and model data. *Phys. Status Solidi (B)* **2011**, *248*, 2857–2863. [CrossRef]
47. Haas, P.; Tran, F.; Blaha, P. Calculation of the lattice constant of solids with semilocal functionals. *Phys. Rev. B* **2009**, *79*, 085104. [CrossRef]
48. Janthon, P.; Luo, S.; Kozlov, S.M.; Viñes, F.; Limtrakul, J.; Truhlar, D.G.; Illas, F. Bulk Properties of Transition Metals: A Challenge for the Design of Universal Density Functionals. *J. Chem. Theory Comput.* **2014**, *10*, 3832–3839. [CrossRef]
49. Henkelman, G.; Arnaldsson, A.; Jónsson, H. A fast and robust algorithm for Bader decomposition of charge density. *Comput. Mater. Sci.* **2006**, *36*, 354–360. [CrossRef]
50. Slater, J.C. Atomic Radii in Crystals. *J. Chem. Phys.* **1964**, *41*, 3199–3204. [CrossRef]
51. Clementi, E.; Raimondi, D.L.; Reinhardt, W.P. Atomic Screening Constants from SCF Functions. II. Atoms with 37 to 86 Electrons. *J. Chem. Phys.* **1967**, *47*, 1300–1307. [CrossRef]
52. Zoberbier, T.; Chamberlain, T.W.; Biskupek, J.; Kuganathan, N.; Eyhusen, S.; Bichoutskaia, E.; Kaiser, U.; Khlobystov, A.N. Interactions and Reactions of Transition Metal Clusters with the Interior of Single-Walled Carbon Nanotubes Imaged at the Atomic Scale. *J. Am. Chem. Soc.* **2012**, *134*, 3073–3079. [CrossRef]
53. Tascón, J.M.D.; Bottani, E.J. Nitrogen Physisorption on Defective C_{60}. *J. Phys. Chem. B* **2002**, *106*, 9522–9527. [CrossRef]
54. Bai, H.; Ji, W.; Liu, X.; Wang, L.; Yuan, N.; Ji, Y. Doping the Buckminsterfullerene by Substitution: Density Functional Theory Studies of C59X (X = B, N, Al, Si, P, Ga, Ge, and As). *J. Chem.* **2013**, *2013*, 9. [CrossRef]
55. Kuganathan, N.; Green, J.C. Mercury telluride crystals encapsulated within single walled carbon nanotubes: A density functional study. *Int. J. Quantum Chem.* **2008**, *108*, 797–807. [CrossRef]
56. Kuganathan, N.; Green, J.C. Crystal structure of low-dimensional Cu(i) iodide: DFT prediction of cuprophilic interactions. *Chem. Commun.* **2008**, *21*, 2432–2434. [CrossRef] [PubMed]
57. Bichoutskaia, E.; Liu, Z.; Kuganathan, N.; Faulques, E.; Suenaga, K.; Shannon, I.J.; Sloan, J. High-precision imaging of an encapsulated Lindqvist ion and correlation of its structure and symmetry with quantum chemical calculations. *Nanoscale* **2012**, *4*, 1190–1199. [CrossRef] [PubMed]